Electron Transport and Back Reaction in Nanocrystalline TiO_2 Films Prepared by Hydrothermal Crystallization

Torsten Oekermann,[†,‡] Dongshe Zhang,[†] Tsukasa Yoshida,*[,†] and Hideki Minoura[†]

Graduate School of Engineering, Environmental and Renewable Energy Systems (ERES) Division, Gifu University, Yanagido 1-1, Gifu 501-1193, Japan, and Institute of Physical Chemistry and Electrochemistry, University of Hannover, Callinstrasse 3-3A, 30167 Hannover, Germany

Received: April 8, 2003; In Final Form: November 6, 2003

The electron transport and back reaction in nanocrystalline TiO_2 films prepared at low temperature using a new hydrothermal crystallization method on conductive glass and plastic substrates have been investigated by intensity modulated photocurrent spectroscopy (IMPS) and intensity modulated photovoltage spectroscopy (IMVS). The hydrothermal method enables the preparation of crack-free TiO_2 thick films and at the same time enhances the electron transport compared to films prepared by low-temperature sintering, providing a path towards efficient photoelectrode materials for flexible dye-sensitized solar cells. UV/ozone treatment of the films enables the removal of residual organics left from the hydrothermal preparation process. Since these organics represent surface states that mediate the back reaction of electrons, the electron lifetime is increased by their removal, while the electron transport is not enhanced significantly. High-temperature sintering of the hydrothermally prepared films leads to both a removal of the surface states and a significant enhancement of the electron transport properties. Interestingly, the electron lifetimes are not changed by high-temperature sintering, since faster electron transport and less surface states have opposite effects on the back reaction process. These films showed improved electron transport properties and efficiencies even if compared with films prepared by conventional high-temperature methods, which shows the high potential for the further development of the hydrothermal method.

Introduction

The highest efficiencies for dye-sensitized solar cells (DSSC) to date have been achieved using porous nanocrystalline TiO_2 electrodes, various Ru complexes as sensitizing dyes, and electrolytes containing the I^-/I_3^- redox couple.[1,2] However, the conventional method for the preparation of TiO_2 electrodes for DSSC using colloidal suspensions of TiO_2 nanoparticles typically includes high-temperature sintering at 450 or 500 °C, which is necessary to remove organic additives used to suppress crack formation and to establish a good connection between the TiO_2 particles. This method, therefore, cannot be applied to prepare films on (flexible) plastic substrates. The development of low-temperature methods to prepare films on such substrates is desirable, because flexible solar cells have a potential for new applications in addition to those with the conventional nonflexible cells used today. Furthermore, polymer foils are easy to handle in processing steps, possibly leading to lower costs in large-scale production.[3]

One method used to prepare nanocrystalline TiO_2 films on plastic substrates so far is low-temperature sintering of TiO_2 colloidal pastes at 100 to 150 °C.[3−5] However, compared to films prepared by high-temperature sintering, significantly lower overall light to electricity conversion efficiencies η have been reported for these films. One reason for the lower efficiencies is because without the use of organic surfactants, only very thin films of about 1 μm thickness could be obtained by the conventional method and subsequent low-temperature sintering,[4] where the low film thickness leads to a low light-harvesting efficiency. A higher film thickness could be obtained by addition of larger TiO_2 particles to the colloidal suspension of TiO_2 nanoparticles[5] or by hydrolysis of $TiCl_4$ and subsequent low-temperature sintering.[6,7] However, in both cases lower electron lifetimes and diffusion coefficients were reported toward lower annealing temperatures,[5,6] which is expected to lead to lower electron diffusion lengths and thus lower electron collection efficiencies of the films.[5] Low electron diffusion coefficients can be caused by a high trap density[5] and/or a low degree of neck growth and electric contact between the particles,[5,7,8] while short electron lifetimes can be caused by a high number of surface states, which are assumed to mediate the back reaction of electrons with I_3^- in the electrolyte.[5,8,9] The usually higher surface area and dye loading of a better crystallized film[6,7] and a possibly stronger adsorption of the dye on a well-crystallized surface, leading to a higher electron injection efficiency,[7] were also suggested as reasons for the higher efficiency of films sintered at high temperature compared to low-temperature films. The most successful low-temperature method to prepare nanoporous TiO_2 films so far proved to be the mechanical compression of TiO_2 powders under high pressure.[10,11] With this method, films with a thickness of up to 8 μm could be obtained, and efficiencies η of up to 3.0% on conductive glass[11] and 2.3% on conductive plastic substrates[10] were reported for a light intensity of 100 mW cm^{-2}.

We have recently developed a new method to prepare nanocrystalline TiO_2 films at a low temperature using a paste that contains nanocrystalline TiO_2 powder, as well as a titanium salt such as $TiCl_4$, $TiOSO_4$, or a Ti(IV) alkoxide. Crystallization of the titanium salts into TiO_2 by hydrothermal treatment in

* Corresponding author. Email: yoshida@apchem.gifu-u.ac.jp.
† Gifu University.
‡ University of Hannover.

10.1021/jp034918z CCC: $27.50
Published on Web 01/21/2004

the gas phase of an autoclave chemically "glues" the TiO_2 particles to form crack-free, robust porous thick films with thicknesses of up to 18 μm at temperatures as low as 100 °C.[12,13] The highest light to electricity conversion efficiency η on indium tin oxide (ITO)-covered plastic substrates was achieved when the films were prepared using titanium isopropoxide ($\eta = 2.3\%$), while such films prepared on fluorine-doped tin oxide (FTO)-covered glass achieved efficiencies of up to 3.1%, both at 100 mW cm^{-2}.[13] These values are comparable to those of films prepared by mechanical compression of TiO_2 powders as mentioned above.[10,11] An even higher efficiency of $\eta = 4.2\%$ on conductive glass could be observed for films prepared by hydrothermal crystallization with $TiCl_4$.[12]

It had already been found earlier that posttreatment of TiO_2 films with $TiCl_4$ leads to an enhanced electron transport in the films, probably through a better connection of the TiO_2 particles.[14,15] Taking this into consideration, the new hydrothermal crystallization method promises to provide an improved electron transport in TiO_2 films even without further heat treatment. We therefore investigated the transport and back reaction kinetics of photogenerated electrons in films prepared by hydrothermal crystallization using intensity modulated photocurrent spectroscopy (IMPS) and intensity modulated photovoltage spectroscopy (IMVS). Films that were prepared using titanium isopropoxide were used in this study, because these films showed the highest efficiency on plastic substrates as mentioned above. Furthermore, films prepared under the same conditions on ITO- or FTO-covered glass, as well as the effects of high-temperature sintering and UV/ozone treatment on these films, were investigated for comparison. The results were also compared with those obtained at TiO_2 films prepared by the conventional high-temperature method using the same TiO_2 nanoparticles. Therefore, this study provides insight into the electron transport and back reaction properties of TiO_2 films prepared by our new method on different substrates, as well as a comparison of TiO_2 films prepared by several different methods, using the same TiO_2 nanoparticles.

Theory

The generation and collection of electrons in dye-sensitized nanocrystalline solar cells can be described by the continuity equation[9,16]

$$\frac{\partial n}{\partial t} = \rho\alpha I_0 \, e^{-\alpha x} + D_n \frac{\partial^2 n}{\partial x^2} - \frac{n - n_0}{\tau_n} \tag{1}$$

where ρ is the efficiency of electron injection, α the absorption coefficient, I_0 the incident light intensity, D_n the effective diffusion coefficient of electrons, τ_n the electron lifetime, n the electron density under illumination, and n_0 the equilibrium electron concentration in the dark. Light scattering in the film and an electric field in the direction of the back contact are assumed to be negligible.[9,17]

During the IMVS and IMPS measurements, the cell is illuminated with sinusoidally modulated light with a small ac component (10% or less of the dc component), which can be described by the periodic illumination function

$$I(t) = I_0[1 + (\delta \, e^{i\omega t})] \tag{2}$$

where ω equals $2\pi f$ and is the variable modulation frequency and $\delta \, I_0$ represents the ac component of the incident photon flux. The photocurrent or photovoltage response is then measured in terms of its amplitude and phase shift with respect to the illumination function, and it can be represented in the IMPS and IMVS complex plane plots.

On the basis of the illumination function in eq 2, analytical solutions of eq 1 for short circuit (IMPS) and open circuit (IMVS) conditions have been published in the literature.[18,19] It was shown that the IMVS response is characterized by a semicircle in the positive/negative quadrant of the complex plane and that τ_n can be calculated directly from the IMVS response by[19,20]

$$\tau_n = \frac{1}{\omega_{\min}} = \frac{1}{2\pi f_{\min}} \tag{3}$$

where $f_{\min}$ is the frequency of the minimum of the semicircle, i.e., the frequency of the lowest imaginary component in the IMVS plot. Correspondingly, the electron transit time

$$\tau_D = \frac{1}{\omega_{\min}} = \frac{1}{2\pi f_{\min}} \tag{4}$$

can be defined for IMPS.[9] Considering a certain penetration depth of the light, this value gives an estimation of the average time that photoinjected electrons need to reach the back contact. It depends on the film thickness and the dye loading of the film. Therefore, τ_D already enables the comparison of the electron transport properties in different films with similar film thickness and dye loading. For a more detailed analysis, the electron diffusion coefficient D_n can be calculated from the IMPS response. This can be done by fitting the IMPS response with the analytical solution of eq 1 for short circuit conditions.[9,18] The normalized solution for the photocurrent j_{photo} and therefore the IMPS response for illumination through the back contact of the film is

$$\frac{j_{\text{photo}}}{q\delta\rho I_0} = \Phi(\omega) = \frac{\alpha}{\alpha + \gamma} \frac{e^{\gamma d} - e^{-\gamma d} + 2\alpha \dfrac{e^{-\alpha d} - e^{-\gamma d}}{\gamma - \alpha}}{e^{\gamma d} + e^{-\gamma d}} \tag{5}$$

with

$$\gamma = \left[\frac{1}{D_n \tau_n} + i\frac{\omega}{D_n}\right]^{1/2} \tag{6}$$

where q is the elementary charge and d is the film thickness. The electron lifetime τ_n, which is necessary for the fitting process, can be directly obtained from separate IMVS measurements at the same film (eq 3). Because a trap-limited electron transport has been found in nanoporous TiO_2,[21,22] the effective diffusion D_n coefficient takes into account the trapping and detrapping of electrons. It can be defined by

$$D_n = D_{\text{cb}} \frac{k_{\text{d}}}{k_{\text{t}}} \tag{7}$$

where k_{t} and k_{d} are the first-order rate constants for the trapping and detrapping, respectively, and D_{cb} is the diffusion coefficient of electrons in the conduction band.[23] Since the trap occupancy is determined by the electron density and thus by the light intensity, a light intensity dependence can also be expected for D_n. However, for small amplitudes of the ac component of the light intensity D_n as well as τ_n can be treated as constant for a given dc light intensity I_0.[18] Out of these two values, the electron diffusion length L_n can then be calculated by the equation

$$L_n = \sqrt{D_n \tau_n} \tag{8}$$

The electron diffusion length is an important factor for a dye-sensitized solar cell, as it should be higher than the film thickness to enable an efficient collection of photogenerated electrons at the back contact.

The experimentally measured IMPS response is affected by *RC* attenuation. To obtain the attenuated response, eq 5 is multiplied with the complex attenuation function

$$A(\omega) = \frac{1}{1 + i\omega RC} \tag{9}$$

where R is the series resistance and C is the capacitance of the electrode.[18] It has been found that, under short circuit conditions, R and C are mainly due to the conducting glass substrate, with typical values of around 10−20 Ω and 30 μF cm^{-2}.[18,24]

Experimental Section

Film Preparation and Characterization. Nanocrystalline TiO_2 powder (0.8 g, Degussa P25) was mixed with 3.6 g of a 1 M ethanolic solution of titanium isopropoxide and stirred for 2 h in a closed vessel to get a viscous paste. The paste was spread on conductive glass coated with F-doped SnO_2 (FTO, 10 Ω/□) or indium tin oxide (ITO, 20 Ω/□) or on conductive flexible plastic substrates (PET) coated with ITO (70 Ω/□). The coated samples were laid on a sample stage placed in an autoclave to which a small amount of pure water was added, so that the samples were not in direct contact with water but with steam during the hydrothermal treatment, which was carried out at 100 °C for 12 h. The films were then dried at 100 °C in an oven for 1 h and immersed in a 0.5 mM ethanolic solution of $Ru(dcbpy)_2(NCS)_2$ (N3 dye, Kojima; dcbpy = 2,2′-bipyridine-4,4′-dicarboxylic acid), where they were kept overnight at room temperature. Details of the preparation process are given elsewhere.[12,13] XRD spectra showed the formation of anatase TiO_2 out of titanium isopropoxide by the hydrothermal treatment.[13]

Optional high-temperature sintering or UV/ozone treatment, in addition to hydrothermal crystallization, was carried out before dye adsorption. If not mentioned otherwise, high-temperature sintering was carried out at 450 °C for 1 h, which was also the case for the films prepared by the conventional method (see below). For UV/ozone treatment, the films were exposed to UV light (λ = 185 and 254 nm) and ozone atmosphere and maintained in a closed chamber under laboratory ambient conditions. The films were placed 6.5 cm from the light source for 2 h. UV light was produced by three mercury-vapor lamps with a light intensity of 4.5 W each (Nippon Laser & Electronics Laboratory NL-UV253), and O_3 was generated (15 mg h^{-1}) by irradiating dry O_2 with the UV light.

For comparison with the hydrothermally prepared films, porous nanocrystalline TiO_2 films were prepared from the same P25 powder according to the conventional high-temperature method published by Grätzel and co-workers.[15] High-temperature sintering and adsorption of the sensitizing dye were carried out as described above.

All films used in this study had a film thickness of about 10 μm. The dye loading of the films was determined by desorbing the dye from the film using 0.1 M ethanolic NaOH solution and measuring its absorption spectrum.[14] The film morphology was observed by a scanning electron microscope (SEM) using a Topcon ABT-150 FS. X-ray photoelectron spectra (XPS) were measured for the C 1s signal using an ESCA-3400 spectrometer (Shimadzu) with the Al Kα X-ray line (1486.6 eV). The spectra were calibrated by using the Ti 2p peak positions (459.5 and 465.2 eV) of the P25 powder as a standard.

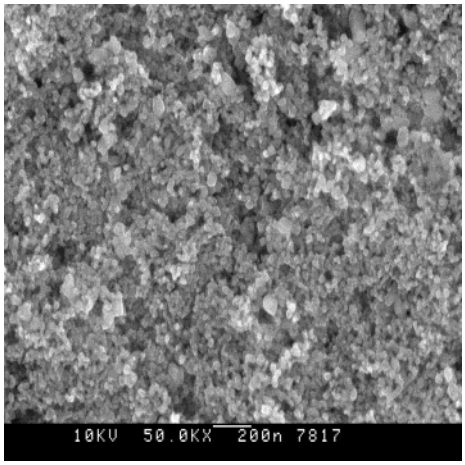

Figure 1. SEM photograph of a TiO_2 film resulted from P25 and titanium isopropoxide ethanol solution after hydrothermal treatment at 100 °C for 12 h.

Photoelectrochemical Measurements. Sandwich cells were made out of the dye-modified TiO_2 electrodes as working electrodes (geometric area of the TiO_2 film ≈ 0.25 cm^2) and platinized FTO on glass as counter electrodes. The electrodes were placed face-to-face without spacer, except for the films on plastic substrate, where small pieces of thin plastic foil (thickness about 10 μm) had to be placed between free parts of the conductive layers of the working electrode and the counter electrode to avoid short-circuiting. The electrolyte was 3-methoxypropionitrile containing 0.5 M LiI, 0.05 M I_2, and 0.5 M *tert*-butylpyridine. Illumination of the cells was carried out through the back contact of the TiO_2 film in all experiments described in this paper.

High-intensity green LEDs (530 nm), which led to a dc light intensity of up to 2.6 mW cm^{-2} at the electrodes, were used as light sources for IMPS and IMVS. The light intensities were modulated (±8%) by modulating the voltage applied to the LED with sinus waves in the frequency range from 0.2 Hz to 10 kHz for IMPS and from 0.02 to 200 Hz for IMVS. The dc and ac light intensities were measured with a calibrated photodiode. Neutral density filters were used to vary the light intensities down to about 0.1 mW cm^{-2}. No corrections were made for absorption and reflection losses in the conductive glass or plastic substrates.

A Toho Technical Research 2000 potentiostat/galvanostat was used to measure the short circuit currents and open circuit voltages. The amplitude and phase shift of the current or voltage response with respect to the modulation of the light intensity were measured with an NF Electronic Instruments S-5720C frequency response analyzer (FRA). The control of the FRA and the data acquisition during a series of measurements was carried out using a personal computer.

Photocurrent action spectra were performed using the same sandwich cell configuration as described above and monochromatic light of different wavelengths with a constant incident photon density of 10^{16} cm^{-2} s^{-1}. The measurements were performed and monitored using a computerized CEP-2000 system (Bunkoukeiki Ltd.).

Results and Discussion

Film Morphology. Figure 1 shows the SEM photograph of a TiO_2 film prepared by hydrothermal crystallization with titanium isopropoxide. The films prepared by this method are highly porous and consist of particles with an average size of ca. 25 nm, which matches the size of the P25 particles used for

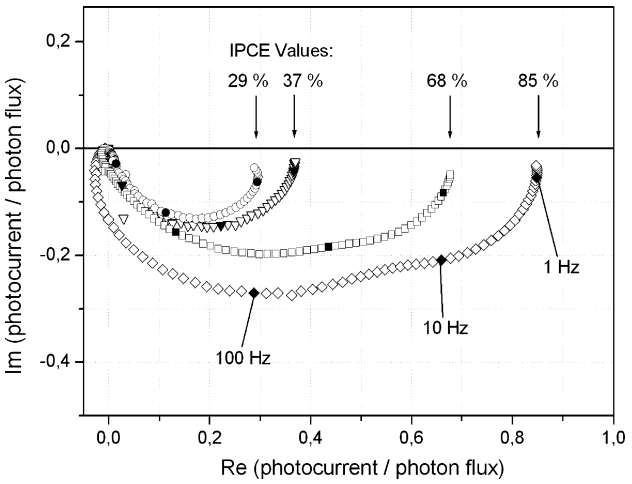

Figure 2. IMPS plots measured with an incident dc light intensity of 2.6 mW cm^{-2} (not considering losses caused by the conductive substrate) for various dye-sensitized TiO_2 films prepared by hydrothermal crystallization (▽ on FTO/glass; ○ on ITO/plastic; ◇ on FTO/glass, sintered at 450 °C for 1 h after preparation). For comparison, the IMPS plot of a film prepared by the conventional method including high-temperature sintering (□) is also shown. The real components of the low-frequency limits represent the IPCE of the films. The respective solid symbols represent the measurements made at 1, 10, and 100 Hz for all films.

their preparation. This suggests that the P25 particles are surrounded by a very thin layer of anatase TiO_2 formed out of the titanium isopropoxide by the hydrothermal treatment. The morphology of the films is actually very similar to that of porous TiO_2 films prepared by the conventional method.[15] This similarity can also be seen in similar dye loadings that could be achieved with the N3 dye. While dye loadings around 1.5×10^{-7} mol cm^{-2} were measured for TiO_2 films prepared by the conventional method in our laboratory, values around 1.3×10^{-7} mol cm^{-2} were obtained for the films prepared by the hydrothermal method. The slightly lower dye loadings for the films prepared by the hydrothermal process can be expected due to a slight smoothing of the internal surface of the films by the additional anatase layer. On the other hand, an influence of the substrate on the film morphology and dye loading was not observed, and these parameters also did not change after subsequent high-temperature sintering at 450 °C.

IMPS Measurements. Typical IMPS complex plane plots can be seen in Figure 2. The plots describe flattened semicircles, caused by a rather broad distribution of electron transit times. Such a broad distribution of electron transit times is expected for illumination through the back contact, since the relative differences in the distances, which photogenerated electrons have to diffuse to reach the back contact, are much higher than for illumination from the electrolyte side. This is also predicted by the IMPS model used in this study.[9,18] Since all films investigated in this study have similar morphologies, dye loadings, and film thicknesses, their distribution of electron transit times should also be similar. Therefore, the values of f_{min} and τ_n (eq 4) already enable a rather good comparison of electron transport properties.

Since the photocurrent divided by the photon flux is shown in Figure 2, the real components of the low-frequency limits of the IMPS plots equal the differential IPCE (incident photon-to-current conversion efficiencies). The differential IPCE values obtained from the IMPS plots are in good accordance with the maximum IPCE values obtained in a number of separate measurements of photocurrent action spectra with a similar light intensity as that used for IMPS (Table 1). It can be seen in Figure 2 that an increasing IPCE is accompanied by an increasing f_{min}, indicating faster electron transport.

TABLE 1. Maximum Incident Photon to Current Conversion Efficiencies (IPCE) for Films Prepared by Hydrothermal Crystallization Using Titanium Isopropoxide (photon number: 10^{16} cm^{-2} s^{-1})

substrate	preparation method	IPCE (%)
ITO/plastic	hydrothermal	33
ITO/glass	hydrothermal	40
FTO/glass	hydrothermal	41
FTO/glass	hydrothermal + sintering	88

A change in the shape of the IMPS plots can be seen especially for the two sintered films which also show the highest IPCE and f_{min}, namely, the film prepared by hydrothermal crystallization and subsequent sintering. This change in the shape also leads to negative real components in the plots toward high frequencies, so that the plots spiral into the origin. Such a change in the shape of the IMPS plots has been shown to be caused by *RC* attenuation as described by eq 9.[24] Since substrates with similar morphology and resistance were used throughout this study and all TiO_2 films had similar geometrical areas, similar *RC* constants for all cells are expected. Therefore, the *RC* attenuation and change in the shape of the IMPS plots become more distinct as f_{min} becomes smaller and as $1/f_{min}$ approaches the value of *RC*. A more detailed analysis of the IMPS plots and the role of *RC* attenuation will be given below.

Compared to the film prepared by the conventional high-temperature method, lower IPCE values are found for the films prepared by the hydrothermal method without sintering. However, it should also be pointed out that these IPCE values, including that for the film prepared on the plastic substrate, compare rather favorably to IPCE values reported in the literature for films prepared by low-temperature sintering.[4] This is in accordance with their higher light-to-electricity conversion efficiencies η as mentioned above.

Another interesting result at this point is the faster electron transport and higher IPCE for the film prepared by hydrothermal crystallization with subsequent high-temperature sintering, compared to the film prepared by the conventional method. Comparable IPCE values near 90% have thus far only been reported for films fabricated by the conventional high-temperature method using pure anatase nanoparticles specially prepared by a hydrothermal synthesis method.[2] These anatase nanoparticles possess a bipyramidal shape, which is indicative of a monocrystalline nature.[8,15] An almost defect-free character expected for such particles should result in faster electron transport and high photocurrents. As mentioned above, a thin anatase layer is also formed during the hydrothermal treatment applied in this study. This should lead not only to a good connection of the P25 particles but also to a curing of surface defects at these particles and thus reduce the electron trap density. Such an effect could account for the rather good performance of the present low-temperature films as compared to other low-temperature films. On the other hand, some amorphous TiO_2 may still be left in the film after the hydrothermal treatment. High-temperature sintering of the hydrothermally prepared films would then lead to a full ripening of the TiO_2 and, by means of the anatase layer, eventually lead to a better connection of the particles and a faster electron transport in these films as compared to conventional high-temperature films. The electron transport properties of the films will be compared and discussed in more detail in the following sections.

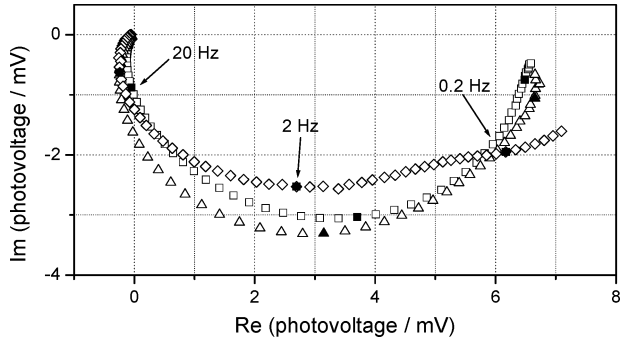

Figure 3. IMVS plots measured with an incident dc light intensity of 2.6 mW cm^{-2} (not considering losses caused by the conductive substrate) for two different dye-sensitized TiO_2 films prepared by hydrothermal crystallization (△ on ITO/glass; ◇ on FTO/glass, sintered at 450 °C for 1 h after preparation). For comparison, the IMVS plot of a film prepared by the conventional method including high-temperature sintering (□) is also shown. The respective solid symbols represent the measurements made at 0.2, 2, and 20 Hz for all films.

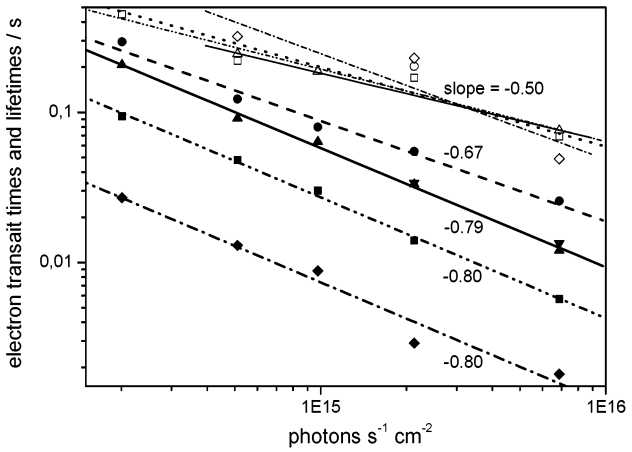

Figure 4. Electron transit times τ_D at different light intensities for various dye-sensitized TiO_2 films prepared by hydrothermal crystallization (▼ on FTO/glass; ▲ on ITO/glass; ● on ITO/plastic; ◆ on FTO/glass, sintered at 450 °C for 1 h after preparation). The respective open symbols show the electron lifetimes τ_n of the films (△ on ITO/glass; ○ on ITO/plastic; ◇ on FTO/glass, sintered at 450 °C). For comparison, the electron transit times (■) and lifetimes (□) of a film prepared by the conventional method, including high-temperature sintering, are also shown. The lines were calculated by linear regression except for the line with a slope of −0.5 (···), which is suggested to represent the electron lifetimes as whole (see text).

IMVS Measurements and Electron Lifetimes. IMVS plots, which were measured at the same light intensity as the IMPS plots shown in Figure 2, are shown in Figure 3. All plots show f_{min} values around 2 Hz, indicating similar electron lifetimes τ_n. A further analysis also showed that the light intensity dependence of τ_n follows the same trend for all films. This can be seen in Figure 4, where the electron lifetimes, which were obtained from IMVS measurements according to eq 3, are plotted against the incident photon number. Figure 4 also shows some linear regression lines for results observed at the same kind of film, respectively, but all results as a whole are represented rather well by a line with a slope of −0.5, which is also shown in this figure. This indicates that τ_n is inversely proportional to the square root of the light intensity. Such a light intensity dependence has already been reported for dye-sensitized nanocrystalline TiO_2,[23] and it can be attributed to a back reaction mechanism of photogenerated electrons with triiodide which is second-order in electron density, assuming that the electron density is proportional to the light intensity.

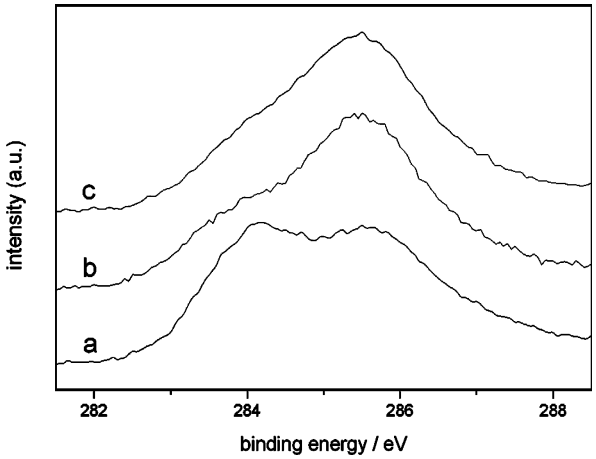

Figure 5. XPS for C1s of porous nanoparticulate TiO_2 films prepared by hydrothermal treatment at 100 °C for 12 h (a) without posttreatment, (b) after UV/ozone treatment, and (c) after sintering at 450 °C for 30 min.

At first view, it is astonishing that no significant differences in the electron lifetimes have been found for films that show such different electron transport properties as seen in the IMPS plots. This is contrary to findings of others that slower electron transport should lead to a longer electron lifetime, since a slower electron transport can indicate a higher trap density, so that electrons spend more time in traps before they can recombine. This has been found experimentally[25] and has also been theoretically and quantitatively discussed in a random walk model of electron transport between trap sites.[26,27]

It should be remembered, however, that other factors such as the density of surface states can influence the electron lifetime, since surface states might mediate the back reaction of electrons with the electrolyte and, therefore, lower the electron lifetime.[5,6,9] As outlined in the following section, XPS measurements (Figure 5) of films prepared by hydrothermal crystallization show the existence of residual organics in the film after the hydrothermal reaction, which probably originates from the titanium isopropoxide and may cause such surface states. The XPS spectra of the films exhibit major peaks assignable to Ti and O (not shown), while small peaks of C1s emission can also be observed, as seen in Figure 5. For the hydrothermally prepared film without posttreatment (Figure 5a) there are two carbon peaks at 284.2 and 285.5 eV. After UV/ozone treatment (Figure 5b) the peak at 284.2 eV diminishes significantly, leaving only a small shoulder. The peak almost completely vanishes after high-temperature sintering of the sample (Figure 5c). On the other hand, no change of the peak at 285.5 eV is observed. The latter peak was already reported by others for TiO_2 films and powders even after treatment by high-temperature sintering,[28,29] and we also found it for the P25 TiO_2 powder used in this study before and after high-temperature sintering (not shown). It was suggested that this peak results from ex situ preparation and transfer processes of the samples.[28] However, the additional peak in the film prepared by the hydrothermal method has not been reported before, and we therefore suggest that it is caused by residual organics from the titanium isopropoxide. From Figure 5, it is evident that the hydrothermal treatment itself cannot remove these organics, while they can be effectively removed by either UV/ozone treatment or high-temperature sintering.

If the residual organics in the films prepared by hydrothermal crystallization represent surface states and these surface states promote the back reaction of electrons as suggested above, their removal should lead to a longer electron lifetime. However,

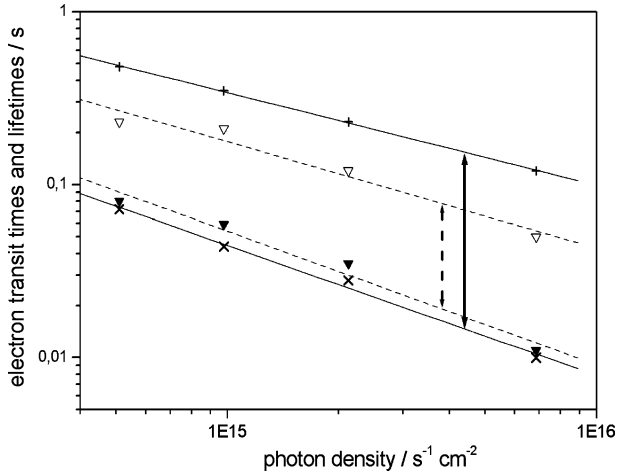

Figure 6. Influence of UV/ozone treatment on the electron transit times τ_D and electron lifetimes τ_n of a film prepared by hydrothermal crystallization on FTO/glass. The values were measured before (- - -, $\tau_D = \blacktriangledown$, $\tau_n = \triangledown$) and after (—, $\tau_D = \times$, $\tau_n = +$) UV/ozone treatment. The lines were calculated by linear regression, and the arrows indicate the difference between τ_D and τ_n before (- - -) and after (—) UV/ozone treatment.

high-temperature sintering not only leads to a removal of the residual organics, but also to a ripening of the TiO_2 and therefore to a faster electron transport as mentioned above, which also influences the electron lifetime. On the other hand, UV/ozone treatment, while it also removes the residual organics, is expected to not significantly influence electron transport in the film. We therefore carried out IMPS and IMVS measurements at a hydrothermally prepared TiO_2 film before and after UV/ozone treatment, and the electron lifetimes and transit times derived from these measurements are shown in Figure 6.

The results before UV/ozone treatment are in very good accordance with the results of the same kind of film in Figure 4, which indicates good reproducibility of the film preparation and photoelectrochemical measurements. After the UV/ozone treatment, the electron transport is only slightly improved as expected, which can be seen in the almost unchanged electron transit times. On the other hand, a significant increase is seen for the electron lifetimes. This is a strong indication that the residual organics, which are removed by the UV/ozone treatment, represent surface states that mainly act as recombination centers. Their removal by UV/ozone treatment leads to longer electron lifetimes because the electron transport is not improved significantly at the same time.

If the surface states are removed by high-temperature sintering (Figure 5c), the electron transport is improved at the same time as seen in the much shorter electron transit times of the hydrothermally prepared film after high-temperature sintering (Figure 4). Less surface states on the one side and faster electron transport on the other side have opposite effects on the electron lifetime. Therefore, it can be understood that films with significantly different electron transport properties can have comparable electron lifetimes in this study, as the lifetime-increasing effect of faster electron transport is compensated by a lower surface state density.

Comparison of Electron Lifetimes and Transit Times. In addition to the electron lifetimes, Figure 4 also shows the electron transit times τ_D, which were calculated from the f_{min} values of the IMPS plots according to eq 4. As expected, a difference of more than 1 order of magnitude is observed between τ_n and τ_D of the film prepared by the conventional method including high-temperature sintering, providing the well-known efficient electron collection in this kind of film. However, the film prepared by hydrothermal crystallization and subsequent sintering even shows a difference of nearly 2 orders of magnitude between τ_n and τ_D, which can be expected to lead to an even higher electron collection efficiency and thus to a higher IPCE (Table 1). The low-temperature films prepared by hydrothermal crystallization without sintering show differences by factors of 6 (glass substrates) and 4 (plastic substrate) between τ_n and τ_D, which still enables the collection of a significant portion of photogenerated electrons even in these relatively thick films, as will be discussed in more detail below.

Except for the film which was prepared on the ITO/plastic substrate, very similar slopes are found for the linear regressions of the transit time data in Figure 4. This is in good accordance with recently published theoretical considerations on the electron transport in dye-sensitized nanocrystalline films in a one-dimensional multiple trapping model in which electron transport is mediated by the conduction band and interrupted by trapping.[30] Assuming an exponential trap distribution and also including the possible back reaction of electrons with tri-iodide, which is second-order in the electron density as shown above, slopes of approximately 0.8 were predicted for plots of $\log(f_{min})$-(IMPS) vs the logarithm of the light intensity I_0. Therefore, a slope of approximately -0.8 is expected for $\log(\tau_n)$ vs $\log(I_0)$, which quantitatively matches most of the data in Figure 4.

The lower modulus of the slope for the film prepared on the plastic substrate indicates a weaker dependence on the light intensity, which may be caused by the involvement of processes which are not light intensity-dependent in first approximation, e.g., slow charge transfer from the TiO_2 to the back contact. In fact, such effects of a slow electron injection into the back contact have already been reported in the literature,[31] and in the case reported here, weaker adhesion of the TiO_2 film on the flexible substrate may be a reason. This would also explain the longer electron transit times for the film prepared by hydrothermal crystallization on ITO/plastic as compared to those on glass substrates, although these electrodes were prepared by the same method and should therefore possess the same electron transport characteristics within the TiO_2 layer. The latter is supported by the fact that the films prepared by hydrothermal crystallization on ITO/glass and FTO/glass do not show significant differences in their electron transit times as seen in Figure 4.

Electron Diffusion Coefficients and Diffusion Lengths. For a more detailed analysis of the electron transport properties, effective diffusion coefficients D_n have been calculated by fitting the IMPS response (see Theory section) for all three kinds of films used in this study on conductive glass substrates. In a first attempt, the D_n values were obtained by best fits with regard to f_{min}, i.e., by inserting experimental data for τ_n, α, and d into the simulation function (eq 5) and then varying D_n manually until a good correspondence with the experimental value of f_{min} was reached. This method was used before by others in IMPS studies on TiO_2/N3 nanoporous films.[32,33] However, the Bode plots in Figure 7 show for a film prepared by the hydrothermal method and subsequent high-temperature sintering that this method gave rather poor fits for the IMPS plots as a whole.

To obtain fits which better represent the experimental curves and also consider the influence of the *RC* constant on the plots which was already seen in Figure 2, eq 5 was multiplied with eq 9, and the result was split into its real and imaginary components as functions of the frequency *f*. Fitting routines for least-squares fits were written for these two functions, and the experimental results were then fitted by simultaneously varying

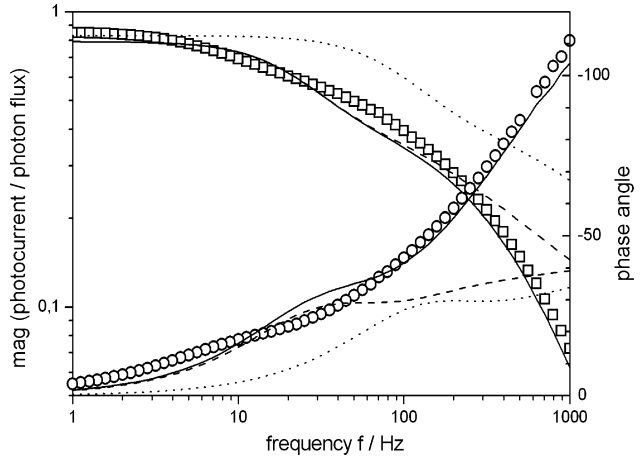

Figure 7. IMPS bode plots (□ magnitude; ○ phase angle) of a dye-sensitized TiO_2 film prepared by hydrothermal crystallization and subsequent sintering at 450 °C for 1 h for an incident dc light intensity of 2.6 mW cm^{-2}. The lines show fits according to eqs 5 and 9 under different conditions (··· best fit with regard to f_{min}, *RC* attenuation neglected; --- least-squares fit, *RC* attenuation neglected; — least-squares fit, including *RC* attenuation with $C = 9\ \mu F$, $R = 37\ \Omega$).

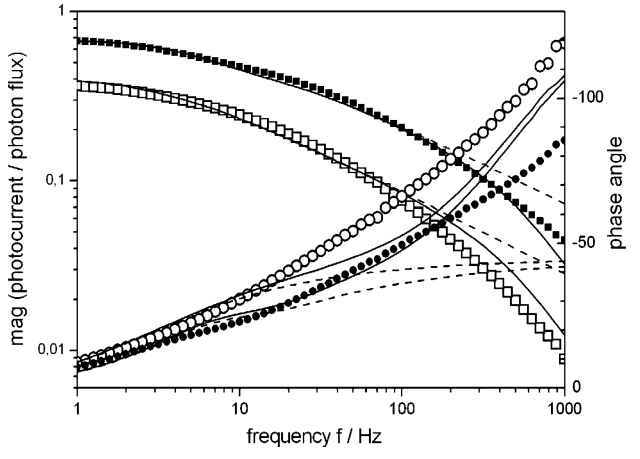

Figure 8. IMPS bode plots of dye-sensitized TiO_2 films prepared by (a) the low-temperature hydrothermal method without posttreatment (□ magnitude; ○ phase angle) and (b) the conventional high-temperature method including sintering at 450 °C (■ magnitude; ● phase angle) for an incident dc light intensity of 2.6 mW cm^{-2}. The lines show least-squares fits according to eq 5 with (—) and without (---) *RC* attenuation according to eq 9. The *R* and *C* values for the fits with *RC* attenuation were 11 μF, 52 Ω for film (a) and 9 μF, 35 Ω for film (b).

D_n, *R*, and *C*, while again experimental data were inserted for τ_n, α, and *d*. To evaluate the role of the *RC* attenuation, fits were also made by varying D_n only and inserting 0 for *R* and *C*, respectively. The example in Figure 7 shows that rather good fits were obtained over the whole frequency range if *RC* attenuation was considered, while significant deviations occurred at higher frequencies if *RC* attenuation was neglected. This clearly shows that the deviations in the IMPS plots, which are seen in Figure 2 toward higher frequencies, are caused by *RC* attenuation. The fits gave values around 10 μF for *C* and 30−40 Ω for *R*. The values for *C* are in very good accordance with the findings of others,[18,24] while the *R* values in our fits, which are about double the values usually reported in the literature, are probably caused by the design of our cells with a rather long distance of about 1−2 cm between the film and the contacts between the conducting glass and the copper wires.

Rather good least-squares fits were also found for the other two kinds of films, as seen in Figure 8. Also, for these two films *RC* attenuation had to be considered in the fitting process to obtain acceptable results. The resulting *R* and *C* values were in the same range as mentioned above for the hydrothermally prepared film with subsequent high-temperature sintering, with higher *R* values of around 50 Ω for ITO/glass substrates due to their lower conductivity (see Experimental Section). This shows a high self-consistency of all the least-squares fits done in the course of this study, which supports the validity of these fits and the resulting D_n values.

The D_n values that were obtained in the fitting process can be seen for different light intensities in Figure 9. As already expected from the low electron transit times (Figure 4), the highest diffusion coefficients are found for the film prepared by hydrothermal crystallization and subsequent high-temperature sintering. Therefore, Figure 9 indicates a significantly enhanced electron transport in this film compared to the film prepared by the conventional high-temperature method in our laboratory. Since the electron lifetime does not change significantly, the enhancement of the electron transport properties then leads to the higher efficiency of the film as outlined above. Accordingly, the films prepared by hydrothermal crystallization without further heat treatment show lower diffusion coefficients as expected from their lower electron transit times.

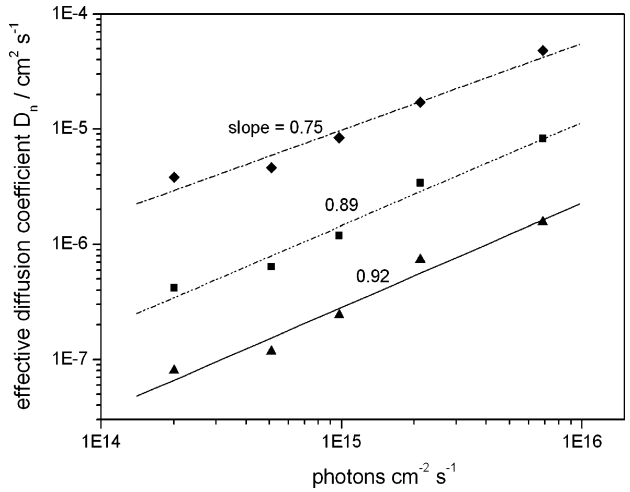

Figure 9. Effective diffusion coefficients D_n at different light intensities for dye-sensitized TiO_2 films prepared by hydrothermal crystallization (▲ on ITO/glass; ◆ on FTO/glass, film sintered at 450 °C for 1 h after preparation). For comparison, the diffusion coefficients of a film prepared by the conventional method including high-temperature sintering (■) are also shown. The D_n values were obtained from least-squares fits of the experimental IMPS results including *RC* attenuation. The lines in the figure were calculated by linear regression.

It should be noted at this point that higher D_n values were obtained when the fits were made with regard to f_{min} only. Compared to the D_n values from least-squares fits, the D_n values from this method were higher by a factor of about 5 for the sintered films and even about 10 for the low-temperature film. In the case of the film prepared by the conventional method, these higher values were in very good accordance with results obtained by others with the same kind of film, using the same experimental and fitting methods.[23,32,33] On the other hand, the least-squares fits seem to give much lower D_n values because other factors such as the different IPCE of the films are considered. In other words, in the least-squares fits D_n is fitted in a way that can explain differences in the performance of the films if the electron injection efficiency is set equal to 1, which is usually the case. Injection efficiencies <1 would lead to higher D_n values in the least-squares fits; thus, the values shown in

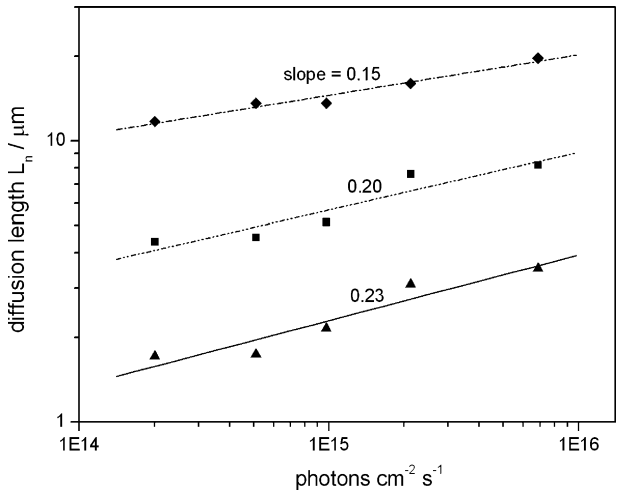

Figure 10. Electron diffusion lengths L_n at different light intensities for dye-sensitized TiO_2 films prepared by hydrothermal crystallization (▲ on ITO/glass; ◆ on FTO/glass, film sintered at 450 °C for 1 h after preparation). For comparison, the diffusion lengths of a film prepared by the conventional method including high-temperature sintering (■) are also shown. The lines were calculated by linear regression.

Figure 9 may be regarded better as a lower limit of the true D_n value, while D_n values obtained from best fits with regard to f_{min} may be regarded as the upper limit of the true D_n value in our study. On the other hand, in least-squares fits of IMPS results in which the electron injection efficiency ρ was varied, ρ mostly reached a value of 1 in the best fits for all three kinds of film. This is an indication that ρ is indeed equal to 1 or close to 1.

The electron diffusion lengths L_n for the three films were calculated according to eq 8 from the data in Figure 9. The results are shown in Figure 10. Note that L_n values of the film prepared by hydrothermal crystallization plus subsequent high-temperature sintering are well above the film thickness of 10 μm, explaining the high efficiency of this film as all photogenerated electrons are collected at the back contact even for the low light intensities used for IMPS and IMVS. L_n values of the film prepared by the conventional high-temperature method are still below 10 μm in this light intensity range, but it has been found before[32,33] and can also be seen in Figure 10 that L_n slowly increases toward higher light intensity, i.e., with higher electron concentration in the conduction band, which leads to a higher trap occupancy and higher D_n. The L_n value which is expected for white light illumination can therefore be estimated from the difference between the photocurrents under IMPS and white light conditions. This difference was found to be at least 1 order of magnitude for all films between illumination with 2.6 mW cm^{-2} (7×10^{15} photons cm^{-2} s^{-1}) green light and 1 sun ($\sim$100 mW cm^{-2}) white light in this study. A diffusion length of at least 14 μm is then estimated from Figure 10 by extrapolation. This lies above the film thickness; however, a certain loss of photogenerated electrons can be expected if a broad distribution of electron transit times as observed earlier in laser-induced time-resolved photocurrent measurements at nanoporous TiO_2 films[34] is considered. Therefore, the differences in the electron transport properties between the two different high-temperature films investigated in this study can be considered a reason for the difference in the performance of these two films.

Rather low L_n values are found for the films prepared by the low-temperature method. On the other hand, they compare rather favorably with diffusion lengths reported in the literature for P25-based TiO_2 films prepared by the conventional method and low-temperature sintering (150 °C). The highest efficiencies for such films thus far have been reported for films where the addition of larger TiO_2 particles allowed the formation of thicker films up to 7 μm, and an electron diffusion length of 2.8 μm for high light intensities (close to 1 sun) was reported for these films.[5] It is seen in Figure 10 that the films prepared by hydrothermal crystallization without heat treatment in this study already reach a comparable diffusion length at a rather low light intensity used in the IMPS measurements (2×10^{15} photons cm^{-2} s^{-1} $\approx$ 0.8 mW cm^{-2}), which causes a much lower electron concentration in the conduction band of TiO_2 as mentioned above. Therefore, compared to the films prepared by the conventional method and low-temperature sintering, enhanced electron transport properties are indicated for the hydrothermally prepared film. Estimating L_n of this film for higher light intensities as suggested above, we obtain a value of 6−7 μm for 1 sun white light illumination. Considering the dye loading of the film, it can be calculated that more than 90% of the incident light with wavelengths near the absorption maxima will be absorbed within this distance. The rather high overall efficiency of the hydrothermally prepared films under white light illumination compared to other low-temperature films (see Introduction) is therefore understood.

Conclusions

Gas-phase hydrothermal treatment of TiO_2 powder with various titanium salts was shown to be a promising method for the preparation of nanocrystalline low-temperature TiO_2 films for dye-sensitized solar cells. The method enables the preparation of rather thick crack-free nanoporous films, increasing the light-harvesting efficiency. At the same time, the method enables an electron transport through the film which is fast enough to collect most of the photogenerated electrons even in these thick films. Both factors are essential for the performance of the film and lead to an increased efficiency compared to TiO_2 films prepared by low-temperature sintering.

In connection with subsequent high-temperature sintering of the films, the efficiency of the films prepared by hydrothermal crystallization surpasses that of films prepared by the conventional high-temperature method using the same TiO_2 nanoparticles. It was shown that this enhancement is related to a significantly enhanced electron transport in the TiO_2 film, which is caused by the good connection of the TiO_2 particles by the additional thin anatase TiO_2 layer. At the same time, no significant change in the electron lifetime was seen after the sintering, which was explained by the removal of residual organics that act as surface states and mediate the back reaction of electrons. The removal of these surface states would lead to a longer electron lifetime and compensates for the effect of the faster electron transport, which would be expected to lead to shorter electron lifetimes.

The significant improvement after high-temperature sintering shows the high potential of the films prepared by the hydrothermal method. To further enhance the electron transport in the low-temperature films and improve their efficiency, investigations on possible methods to further improve the electron collection efficiency of low-temperature films without applying high temperatures are currently underway. Already in this article, it has been shown that UV/ozone treatment could be one such method, because it can remove residual organics from the films, which leads to a higher electron lifetime. A detailed study on the UV/ozone treatment and its influence on the efficiency of nanoporous TiO_2 films will be the topic of a separate article.

Acknowledgment. The present study received financial support from the Industrial Technology Research Grant Program in 2002, the New Energy and Industrial Technology Development Organization (NEDO) of Japan (01B64002c), and Grant-in-Aid for Scientific Research from the Ministry of Education, Culture, Sports, Science and Technology of Japan (15681005). Postdoctoral fellowships and additional research funds for T.O. and D.Z. from the Japan Society for the Promotion of Science (JSPS) are gratefully acknowledged. We are also grateful for the careful review and suggestions of one of the reviewers which were helpful to achieve detailed analysis of the IMPS results.

References and Notes

(1) O'Regan, B.; Grätzel, M. *Nature* **1991**, *353*, 737.
(2) Grätzel, M. *Nature* **2001**, *415*, 338.
(3) Sommeling, P. M.; Späth, M.; Kroon, J.; Kinderman, R.; Van Roosmalen, J. In *16th European Photovoltaic Solar Energy Conference*, Proceedings of the International Conference, Glasgow, U.K., May 1−5, 2000; Scheer, H., Ed.; James & James Science Publishers: London, 2001; pp 67−71, Vol. 1.
(4) Pichot, F.; Pitts, J. R.; Gregg, B. A. *Langmuir* **2000**, *16*, 5626.
(5) Nakade, S.; Matsuda, M.; Kambe, S.; Saito, Y.; Kitamura, T.; Sakata, T.; Wada, Y.; Mori, H.; Yanagida, S. *J. Phys. Chem. B* **2002**, *106*, 10004.
(6) Park, N. G.; Schlichthörl, G.; van de Lagemaat, J.; Cheong, H. M.; Mascarenhas, A.; Frank, A. J. *J. Phys. Chem. B* **1999**, *103*, 3308.
(7) Kim, K.-J.; Benkstein, K. D.; van de Lagemaat, J.; Frank, A. J. *Chem. Mater*. **2002**, *14*, 1042.
(8) Park, N.-G.; van de Lagemaat, J.; Frank, A. J. *J. Phys. Chem. B* **2000**, *104*, 8989.
(9) Peter, L. M.; Vanmaekelbergh, D. In *Advances in Electrochemical Science and Engineering*; Alkire, R. C., Kolb, D. M., Eds.; Wiley-VCH: Weinheim, Germany, 1999; Vol. 6.
(10) Lindström, H.; Holmberg, A.; Magnusson, E.; Lindquist, S.-E.; Malmqvist L.; Hagfeldt, A. *Nano Lett.* **2001**, *1*, 97.
(11) Lindström, H.; Magnusson, E.; Holmberg, A.; Södergren, S.; Lindquist, S.-E.; Hagfeldt, A. *Sol. Energy Mater. Sol. Cells* **2001**, *73*, 91.
(12) Zhang, D.; Yoshida, T.; Minoura, H. *Chem. Lett*. **2002**, 874.
(13) Zhang, D.; Yoshida, T.; Minoura, H. *Adv. Mater.* **2003**, *15*, 814.
(14) Nazeeruddin, M. K.; Kay, A.; Rodicio, I.; Humphry-Baker, R.; Müller, E.; Liska, P.; Vlachopoulos N.; Grätzel, M. *J. Am. Chem. Soc*. **1993**, *115*, 6382.
(15) Barbé, C. J.; Arendse, F.; Comte, P.; Jirousek, M.; Lenzmann, F.; Shklover, V.; Grätzel, M. *J. Am. Ceram. Soc*. **1997**, *80*, 3157.
(16) Södergren, S.; Hagfeldt, A.; Olsson, J.; Lindquist, S. E. *J. Phys. Chem.* **1994**, *95*, 5522.
(17) Vanmaekelbergh, D.; de Jongh, P. *J. Phys. Chem. B* **1999**, *103*, 747.
(18) Dloczik, L.; Ileperuma, O.; Lauermann, I.; Peter, L. M.; Ponomarev, E. A.; Redmond, G.; Shaw, N. J.; Uhlendorf, I. *J. Phys. Chem. B* **1997**, *101*, 10281.
(19) Schlichthörl, G.; Huang, S. Y.; Sprague, J.; Frank, A. J. *J. Phys. Chem. B* **1997**, *101*, 8141.
(20) Franco, G.; Gehring, J.; Peter, L. M.; Ponomarev, E. A.; Uhlendorf, I. *J. Phys. Chem. B* **1999**, *103*, 692.
(21) de Jongh, P. E.; Vanmaekelbergh, D. *Phys. Rev. Lett.* **1996**, *77*, 3427.
(22) Vanmaekelbergh, D.; de Jongh, P. E. *Phys. Rev. B* **2000**, *61*, 4699.
(23) Fisher, A. C.; Peter, L. M.; Ponomarev, E. A.; Walker, A. B.; Wijayantha, K. G. U. *J. Phys. Chem. B* **2000**, *104*, 949.
(24) Franco, G.; Peter, L. M.; Ponomarev, E. A. *Electrochem. Commun.* **1999**, *1*, 61.
(25) Haque, S. A.; Tachibana, Y.; Willis, R. L.; Moser, J. E.; Grätzel, M.; Klug, D. R.; Durrant, J. R. *J. Phys. Chem. B* **2000**, *104*, 538.
(26) Nelson, J. *J. Phys. Rev. B* **1999**, *59*, 15374.
(27) Scher, H.; Montroll, E. W. *Phys. Rev. B* **1975**, *12*, 2455.
(28) Liu, G.; Jaegermann, W.; He, J.; Sundström, V.; Sun, L. *J. Phys. Chem. B* **2002**, *106*, 5814.
(29) Sasaki, T.; Ebina, Y.; Fukuda, K.; Harada, M.; Watanabe, M. *Chem. Mater*. **2002**, *14*, 3524.
(30) Kambili, A.; Walker, A. B.; Qiu, F.; Fisher, A. C.; Savin, A. D.; Peter, L. M. *Physica E* **2002**, *14*, 203.
(31) de Jongh, P. E.; Meulenkamp, E. A.; Vanmaekelbergh, D.; Kelly, J. J. *J. Phys. Chem. B* **2000**, *104*, 7686.
(32) Peter, L. M.; Wijayantha, K. G. U. *Electrochem. Commun*. **1999**, *1*, 576.
(33) Peter, L. M.; Wijayantha, K. G. U. *Electrochim. Acta* **2000**, *45*, 4543.
(34) Solbrand, A.; Lindström, H.; Rensmo, H.; Hagfeldt, A.; Lindquist, S.-E. *J. Phys. Chem. B* **1997**, *101*, 2514.